START PAGE

Chapter 14

LARGE POWER DRIVES

14.1. POWER AND SPEED LIMITS: MOVING UP

Large power drives are defined as those drives beyond the reach of low voltage (up to 660V a.c. source) PWM voltage source inverters with IGBTs (and high switching frequency). The two level IGBT-inverter power limit per unit has increased steadily in the last decade to about 2MW (at the time of this writing) by paralleling four 500kW units. With respect to voltage level, we have noted the introduction of 3 to 5 IGBT power cells (diode rectifier plus single phase PWM inverter) in series per phase — properly insulated from each other and to ground — to supply 1MW and more a.c. motors at line voltages up to 4.5kV (rms) [1].

So powers above 1-2MW, where GTO or thyristor power electronic converters are a must, may be termed as large powers. High powers per unit have been achieved with thyristor rectifier-current source inverter synchronous motors: 100MW for speeds up to 3000rpm, 30MW at 6000rpm, 3MW at 18000rpm. In low speed applications, such as cement mills (up to 20rpm, 5-6Hz) and up to 11MW power [2], thyristor cycloconverter-synchronous motor drives are predominant.

Recently, 3 level GTO voltage source inverters (at 15MW, 60Hz and 6kV line voltage [rms]) for synchronous motor drives have been introduced for steel main rolling mills [3]. It seems that this new breakthrough will drastically change the large power drives' technologies spectrum. For limited speed control (±20% around rated speed) doubly fed induction motor drives with a step down transformer-cycloconverter supplying the rotor circuit have been built for powers up to 400MW for pumped-storage hydropower plants. In such applications, the motoring is used during off-peak energy consumption hours for pumped storage and generating is used during peak hours [4]. Variable speed is useful to reduce energy consumption during motoring and extract energy at maximum available hydroturbine efficiency during generating mode.

The rotor converter power is proportional to speed control ratio (up to 20%) and so are the costs. Resistive starting for motoring is still required.

Note: By now, electric or diesel-electric multimotor propulsion systems for powers up to 6MW are provided with 2 level GTO (IGBT in the future) voltage-source inverters and induction motors or with cycloconverters and induction (or synchronous motors) or with thyristor controlled rectifier current inverters. For ship electric propulsion cycloconverters-synchronous

motor drives at low speed prevail. Note that all these solutions are similar to those mentioned above for large power drives.

A recent newcomer to the field is the diode rectifier-voltage source inverter with insulated gate commutated thyristor (IGCT) for powers up to 5MW at 4.16kV. Finally, a multilevel active front bidirectional PWM converter synchronous motor drives at 50 MW/unit and at 60 KV (with cable made high voltage stator winding) has been dedicated very recently in a gas compressor submarine application. Six main large power drive technologies are summarized in Table 14.1.

Table 14.1. Large power drives

Power flow	bidirectional	bidirectional	bidirectional	bidirectional	unidirectional	unidirectional
Power quality	unity power factor, low line harmonics, high efficiency through regenerative GTO snubbers	rather low power factor	low power factor and high line current harmonics at low speed unity power factor and low line current harmonics	rather low power factor though stator active and reactive power control is possible	low power factor	Close to unity source side power factor: it needs strong input current + filter (transformer)
Speed range	6 Hz	6 Hz	120 Hz(6000 rpm) 60 Hz(3600 rpm) 300 Hz(18000 rpm) Up to 300 Hz	Frequency: ± 20Hz variable, in the rotor; 50 (60)Hz constant in the stator	60 Hz	3000 rpm
Power range	10MVA (15VA / 1 minute)	10MW	30 MW 100 MW 3 MW 1 - 4 MW	Up to 100 - 200 MVA	Up to 10 MW or more	5 MW 4 KV

Motor type	synchronous (without rotor damper winding)	synchronous (without rotor damper winding)	synchronous (with rotor damper winding) induction synchronous (with rotor damper winding)	doubly fed induction motor	doubly fed induction motor	cage rotor induction motors
Converter type	3 level GTO rectifier – voltage source inverter	Thyristor cycloconverter	Rectifier – current source inverter a.) with thyristors b.) with GTOs	Step down transformer and cycloconverter in the rotor circuit	Diode rectifier current source inverter and transformer in the rotor circuit	Diode rectifier current source inverter with integrated gate commutated thyristors

14.2. VOLTAGE SOURCE CONVERTER SYNCHRONOUS MOTOR DRIVES

Both the 3-level GTO inverters and the cycloconverters are, in fact, voltage source type PECs with load current control and they drive the excited rotor synchronous motor at the unity power factor, above 5% of rated speed. Being both a voltage source type, the SM rotor may be cageless which is a notable simplification with sizeable motor costs reduction.

Also, the vector control system of cycloconverter is similar to that of PWM-IGBT converter. There are major differences related to the fundamental output frequency limit, which is $f_1/3$ for the standard cycloconverter.

In contrast, the voltage source inverter is limited in frequency only by the switching frequency in the converter which, for large power GTOs, is, today, around 300Hz.

Also, the cycloconverter is notably less expensive but the power factor, especially at low motor frequencies (well below the rated one) is rather low.

A 3-level GTO inverter system is shown on Figure 14.1.

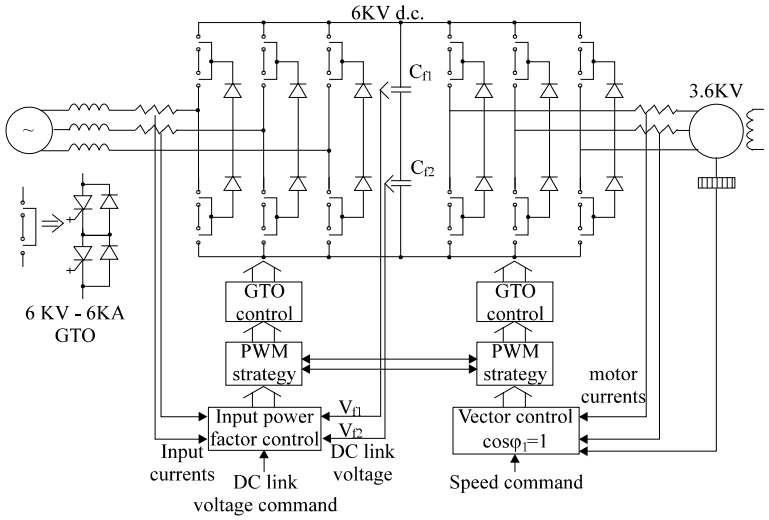

Figure 14.1. A 3-level GTO inverter - SM drive

To reduce the losses in the GTOs a regenerative snubber circuit topology is used. Space vector voltage PWM techniques are applied to improve the motor current waveform, taking advantage of the three-level voltage available in the d.c. link circuit.

Unity power factor control for the motor side and on the source side may be performed through DC link voltage (filter capacitor voltage) control.

A high power cycloconverter SM drive configuration is shown in Figure 14.2.

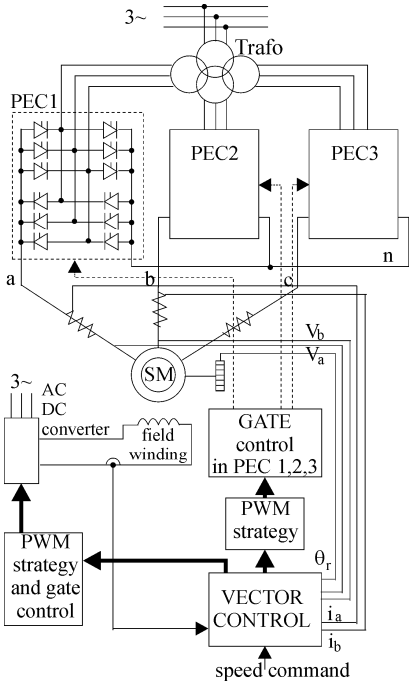

Figure 14.2. A cycloconverter SM drive.

Each phase is fed from a double rectifier bridge — one for each current polarity — to produce operation in 4 quadrants (positive and negative output voltage and current) with phase angle control. The output voltage waveform is "carved" from a sequence of adequate (same polarity, highest value) sections of the three-phase voltage waveforms of the input source and constant frequency f_1 (Figure 14.3).This is why the output frequency is a fraction of the input frequency.

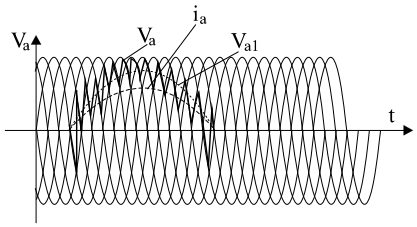

Figure 14.3. Output voltage V_a, and ideal current i_a of the cycloconverter for unity power factor operation of SM

The motor current waveform is rather close to a sinusoid, while the voltage waveform (consequently the motor flux) has harmonics whose order is related to the ratio between the output frequency f_2 and input frequency f_1.

Theoretically, $f_{2max} = f_1 / 2$. Unfortunately, the input currents are closer to rectangular waveforms (Figure 14.4) and are not even fully symmetric.

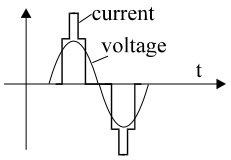

Figure 14.4. Input phase voltage and current of cycloconverters

A lagging power factor is obtained as the thyristors are line (input source) commutated.

To decouple the thyristor commutation process of three phases, the leakage inductance of the source side transformer has to be concentrated mostly in its secondary.

The line current harmonics and the input lagging power factor (lower at lower motor speeds) are serious demerits of the otherwise rather simple and rugged cycloconverter configuration.

Now since the cycloconverter is also a voltage source, as the 3-level GTO inverter system is, vector control of both is similar, though, in general, the first one is applied for low frequency drives ($f_2 < 6$Hz) and the second one for up to 60Hz (or more, as required).

14.3. VECTOR CONTROL IN VOLTAGE SOURCE CONVERTER SM DRIVES

In essence, vector control of SMs is performed either in d-q rotor coordinates or in stator flux coordinates. The d-q model equations for a salient pole cageless rotor SM is (Chapter 10)

$$\bar{V}_s = r_s \bar{i}_s + \frac{d\bar{\lambda}_s}{dt} + j\omega_r \bar{\lambda}_s \tag{14.1}$$

$$\bar{\lambda}_s = \lambda_d + j\lambda_q;\ \ \bar{i}_s = i_d + ji_q;\ \ \bar{V}_s = V_d + jV_q; \tag{14.2}$$

$$\lambda_d = L_d i_d + L_{dm}(i_d + i_F);\ L_d = L_{dm} + L_{sl} \tag{14.3}$$

$$\lambda_q = L_q i_d;\ L_q = L_{qm} + L_{sl} \tag{14.4}$$

$$\frac{d\lambda_F}{dt} = V_f - r_f i_F \tag{14.5}$$

$$T_e = \frac{3}{2} p\left(\lambda_d i_q - \lambda_q i_d\right) \tag{14.6}$$

$$\frac{J}{p}\frac{d\omega_r}{dt} = T_e - T_{load} \tag{14.7}$$

For steady-state (d/dt=0) and unity power factor the space vector diagram (from equations (14.1)-(14.4)) is as shown in Figure 14.5.

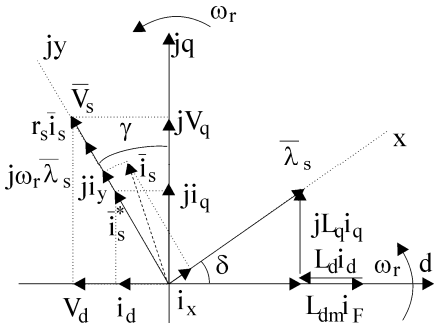

Figure 14.5. Space vector diagram of SM at steady-state and unity power factor ($\varphi_1 = 0$)

During the vector control process the stator current space vector $\bar{i}_s$ differs from the reference space vector $\bar{i}_s^*$. Consequently, the actual current $\bar{i}_s$ may be written in flux (M, T) coordinates

$$\bar{i}_s = i_M + ji_T \tag{14.8}$$

Evidently, for unity power factor (zero angle, φ_1, between $\bar{V}_s^*$ and $\bar{i}_s^*$) i_M should be zero. In reality, during transients at least, as the field current i_F correction is rather slow (to maintain constant stator flux), the unity power factor condition is abandoned for a short time and a nonzero value of i_M is referenced.

How to calculate, approximately, a reference flux current i_M^* is not simple unless the motor has a nonsalient rotor: $L_d = L_q$. Let us calculate the torque from (14.6) and (14.3)-(14.4)

$$T_e = \frac{3}{2}p\left[L_{dm}i_F + \left(L_d - L_q\right)\cdot i_d\right]\cdot i_q \tag{14.9}$$

As $L_d \geq L_q$ and $i_d < 0$ (demagnetizing effect, for unity power factor) the reluctance torque (small as it may be) will be negative. *So it would be adequate to use a cageless nonsalient pole rotor SM*. This is possible in 2(4)-pole rotors used in high speed applications, but it seems still possible for a 5-6Hz, 4(6) multi-pole rotor, 11MW SM where the rotor pole pitch is 0.66m.

The stator flux may be written as:

$$\lambda_s^* = L_{dm}i_M^* \tag{14.10}$$

$$i_M^* \approx i_F \cos\delta + i_x^* \cdot \frac{L_d}{L_{dm}} \tag{14.11}$$

where

is strictly valid for $L_d = L_q$.

For $L_d = L_q$ the torque from (14.6) is

$$T_e = \frac{3}{2} p\left(\lambda_d i_q - \lambda_q i_d\right) \tag{14.12}$$

$$i_T^* = \frac{T_e^*}{\frac{3}{2} p \lambda_s^*} = i_y^* \tag{14.13}$$

with

From (14.11) we may calculate

$$i_x^* = \left(i_M^* - i_F \cos\delta\right) \frac{L_{dm}}{L_d} \tag{14.14}$$

The stator flux has to be controlled directly through the field current control. But first the stator flux has to be estimated.

We again resort to the combined voltage (in stator coordinates) and current model (in rotor coordinates)

$$\hat{\bar{\lambda}}_{sv}^{\,s} = \int \left(\bar{V}_s - r_s \bar{i}_s\right) dt + \bar{\lambda}_{s0} \tag{14.15}$$

$$\hat{\bar{\lambda}}_{si}^{\,r} = L_{sl} i_d + L_{dm}\left(i_d + i_F\right) + j L_q i_q \tag{14.16}$$

$$\hat{\bar{\lambda}}_s = \hat{\bar{\lambda}}_{sv} \cdot \frac{T_c}{1 + sT_c} + \hat{\bar{\lambda}}_{si}^{\,r} e^{j\theta_{er}} \frac{1}{1 + sT_c} \tag{14.17}$$

For low frequencies, the current model prevails while at high frequency, the voltage model takes over. If only short periods of low speed operation are required, the current model might be avoided, by using instead the reference flux λ_s^* in stator coordinates

$$\hat{\bar{\lambda}}_s = \hat{\bar{\lambda}}_{sv} \cdot \frac{T_c}{1 + sT_c} + \lambda_s^* e^{j\theta_{er}} \frac{1}{1 + sT_c} \tag{14.18}$$

$$\sin\left(\theta_{er} + \delta\right) = \frac{\mathrm{Im\,ag}\,\hat{\bar{\lambda}}_s}{\left|\hat{\bar{\lambda}}_s\right|}; \quad \cos\left(\theta_{er} + \delta\right) = \frac{\mathrm{Re}\,\hat{\bar{\lambda}}_s}{\left|\hat{\bar{\lambda}}_s\right|}; \tag{14.19}$$

with θ_{er} measured, δ may be found (Figure 14.5).

Finally, the vector current control in stator flux coordinates is shown in Figure 14.6.

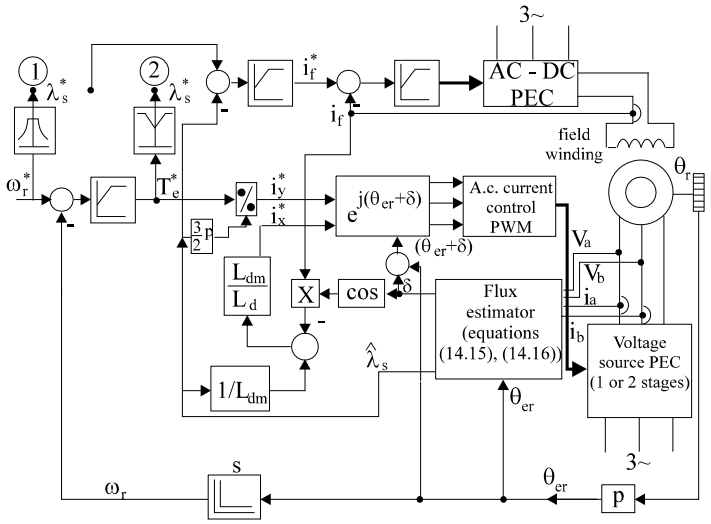

Figure 14.6. Vector current control of SM fed from voltage source type (1 or 2 stages) PECs and unity power factor

The kind of direct vector current control system shown in Figure 14.6 "moves" most of parameter dependence problems into the flux estimator but relies heavily on the rotor position feedback (a resolver is used generally).

Voltage decoupling is not considered but it could be handled as for PM-SM drives when d.c. current (i_x, i_y) controllers are used and the motion induced voltage is added only along axis y

$$V_x^* = 0 \tag{14.20}$$

$$V_y^* = \omega_r \lambda_s \tag{14.21}$$

In this case, open-loop (voltage) PWM is performed (Figure 14.7).

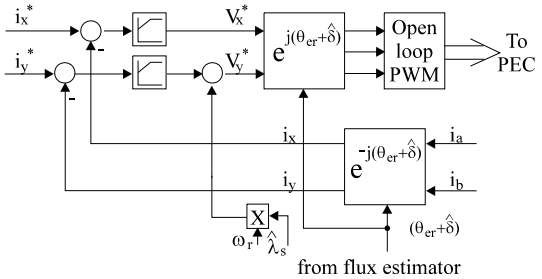

Figure 14.7. Voltage decoupler in stator flux coordinates and d.c. current controllers

The voltage decoupler with d.c. current controllers is known to give better performance around and above rated frequency (speed) and to be less sensitive to motor parameter detuning. Flux control as done in Figure 14.6.

proved to provide fast response in MW power motors due to the delay compensation by nonzero transient flux current reference i_x^*.

Also, fast speed control and reversal has been proved practical with vector current control.

In drives where the load is dependent only on speed the reference flux switch is on 1 (Figure 14.6), while it is on position 2 where the torque may vary at any speed. The flux level has to increase with torque to preserve the unity power factor with variable load.

Response frequency of more than 600rad/s in torque and speed control has been reported for a 11MW drive with a 3-level GTO inverter system [3]. Similar results have been obtained with a 2500kW cycloconverter SM drive [6].

Besides vector current control with voltage decoupler, direct torque and flux control (DTFC) for the unity power factor may be performed to obtain a simpler and more robust control while preserving quick response.

14.4. DIRECT TORQUE AND FLUX CONTROL (DTFC)

Vector current control, as discussed in the previous paragraph, is performing direct flux control but it does not do direct torque control. Also it uses current vector rotators.

The stator flux estimator equations (14.15-14.19) could easily be augmented to also perform torque estimation (Figure 14.8).

For the unity power factor, the angle between stator flux and current is 90°. Also, a reactive torque RT is defined as

$$RT = Q_1 / \omega_1 \tag{14.22}$$

where Q_1 is the reactive power and ω_1 the primary frequency.

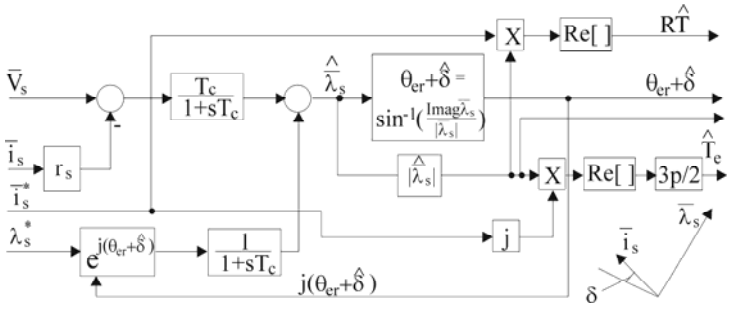

Figure 14.8. Flux and torque observer

The reactive torque RT may be estimated from (14.15) and works well for steady-state and above 5% of rated speed. To make sure that the power factor is unity, the $\hat{RT}$ should be driven to zero through adding or

subtracting from reference field current (Figure 14.9). Finally, we should remember that the torque and flux error and stator flux position in one of the 60° wide sectors solely lead to a voltage vector (or a combination of) in the PEC, to form the table of optimal switching (and timings) as in any DTFC system. The table of optimal switchings (TOS) remains the same as for IMs or PM-SMs. Consequently, the DTFC system is as in Figure 14.9.

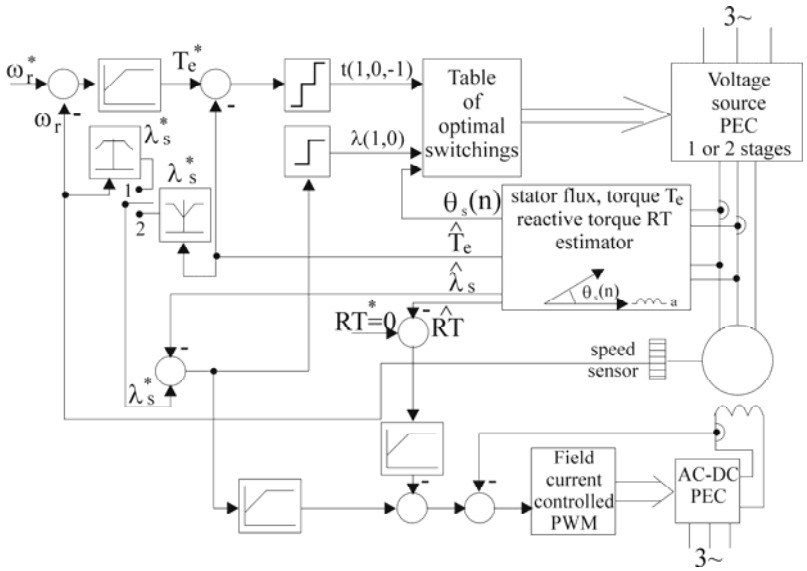

Figure 14.9. DTFC of voltage source PWM converter SM drives

A prompt start up process requires the flux to be present in the machine. To do so, first we initiate the field current control while the stator is fed through a zero voltage vector until the stator flux λ_s surpasses the reference flux for the first time. After that, the motor may start.

14.4.1. Sensorless control

We should note that the rotor position is not present directly in the DTFC scheme but rotor speed is. Consequently, for sensorless control, a rotor speed estimator is required. We may define rotor speed $\hat{\omega}_r$ as:

$$\hat{\omega}_r = \hat{\omega}_1 - \frac{d\hat{\delta}}{dt};\quad \omega_1 = \frac{d\hat{\theta}_s}{dt};\quad \hat{\theta}_s = \sin^{-1}\left(\frac{\mathrm{Imag}\,\hat{\bar{\lambda}}_s}{\left|\hat{\bar{\lambda}}_s\right|}\right) \tag{14.23}$$

where $\hat{\bar{\lambda}}_s$ is the stator flux; $\hat{\omega}_1$, space vector speed, and $\hat{\delta}$ is flux vector angle with respect to rotor d axis.

To a first approximation ($L_d = L_q$) for $\cos\varphi_1 = 1$ the torque is (14.9)

$$\hat{T}_e = \frac{3}{2} p L_{dm} i_F i_q \approx \frac{3}{2} p L_{dm} i_F i_s \cos\delta \tag{14.24}$$

with

$$\text{sign}\left(\cos\hat{\delta}\right) = \text{sign}\left(\hat{T}_e\right) \tag{14.25}$$

So

$$\cos\hat{\delta} \approx \frac{2\hat{T}_e}{3pL_{dm} i_F i_s}; \quad \sin\hat{\delta} = \sqrt{1-\cos^2\hat{\delta}} \tag{14.26}$$

i_F and i_s are measured and L_{dm} has to be known.

Consequently,

$$\frac{d\hat{\delta}}{dt} = \cos\hat{\delta}\frac{d\left(\sin\hat{\delta}\right)}{dt} - \sin\hat{\delta}\frac{d\left(\cos\hat{\delta}\right)}{dt} \tag{14.27}$$

Equation (14.27) may represent an estimator for $\frac{d\hat{\delta}}{dt}$. On the other hand, the stator flux speed $\hat{\omega}_1$ is as shown in Chapter 11

$$\hat{\omega}_1 = \frac{\hat{\lambda}_{s\alpha}(k-1)\cdot\hat{\lambda}_{s\beta}(k) - \hat{\lambda}_{s\beta}(k-1)\cdot\hat{\lambda}_{s\alpha}(k)}{\left|\bar{\lambda}_s\right|^2 T} \tag{14.28}$$

where T is the sampling time.

Using (14.28) in (14.27)

$$\frac{d\hat{\delta}}{dt} = \left(\cos\hat{\delta}(k-1)\sin\hat{\delta}(k) - \sin\hat{\delta}(k-1)\cos\hat{\delta}(k)\right)/T \tag{14.29}$$

As expected, for steady-state the angle $\hat{\delta}$ is constant and thus $\frac{d\hat{\delta}}{dt} = 0$.

14.5. LARGE MOTOR DRIVES: WORKING LESS TIME PER DAY IS BETTER

Large power drives do not work, in general, 24 hours a day, but many times they come close to this figure. Let us suppose that a cement mill has a

5MW ball mill drive that works about 8000 hours/year, that is, about 22 hours/day (average) for 365 days and uses 45000MWh of energy.

A 16MW drive would work for 4000 hours to consume about 44000MWh (not much less). However, the 16MW drive may work only off peak hours.

The energy tariffs are high for 6 hours (0.12$/kWh), normal for 8 hours (0.09$/kWh) and low for 10 hours (0.04$/kWh).

As the high power drive works an average of 11hours/day/365 days (or 12 hours/day excluding national holidays), it may take advantage of low tariff for 10 hours and work only 2 hours for normal tariff..

The lower power drive, however, has to work at least 4 peak tariff hours. Though the energy consumption is about the same, the cost of energy may be reduced from $3,700,000 to $1,700,000 per year, that is more than 50%.

As investment costs are not double for doubling the power (60% more) and the maintenance costs are about the same, the revenue time is favorable for the higher power drive working less time per day.

14.6. RECTIFIER-CURRENT SOURCE INVERTER SM DRIVES - BASIC SCHEME

Standard high speed (50(60)Hz or more) large power variable speed SM drives, traditionally above only 750kW, use rectifier-current source inverters (CSI). Load commutation of thyristors is required. The SMs are capable of leading power factor angle, $\varphi_1 = -(6°-8°)$, and thus, above 5% of rated speed, load commutation is feasible.

Both the phase-delay rectifier (PDR) and the CSI make use of thyristors and thus they may be built at low costs.

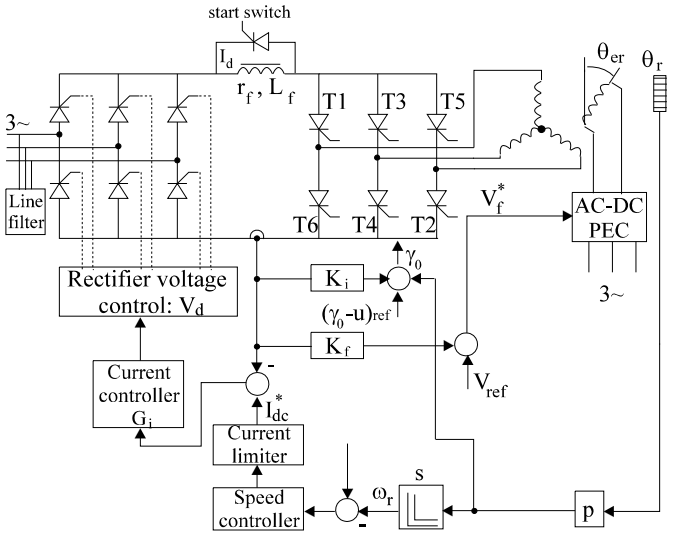

Figure 14.10. Basic scheme of Rectifier - CSI-SM drive

To reduce torque pulsations at low speed, PWM (current notches) of the otherwise rectangular (120° wide) currents may be used.

Here we introduce the basic scheme (Figure 14.10), steady-state equations and performance with load commutation and an advanced control scheme which provides constant leading power factor with load and speed response without overshooting.

The basic scheme of the rectifier-CSI-SM drive in Figure 14.10 uses an indirect vector current control scheme and contains:

- a fully controlled (phase-delay) rectifier;
- a current choke (r_f, L_f);
- a CSI-load commutated;
- a rotor position sensor (γ_0) or a terminal voltage zero crossing sensor (γ);
- advance angle (γ and γ_0 increasing with load (I_{dc})) controller for constant leading power factor angle and safe commutation (limited overlapping angle u);
- speed controller with current limiter;
- d.c. current controller;
- an a.c.-d.c. PEC for the field winding.

The CSI provides only the synchronization between the rotor position and stator current 120°-wide blocks through the advance angle $\gamma_0(\gamma)$.

The controlled rectifier modifies the d.c. link (and stator) current level, that is the torque, in order to perform speed control.

The d.c. link voltage produced by the rectifier V_d is positive for motoring and negative for generating. Through proper changing of the inverter firing sequence, regenerative braking and speed reversal are obtained. Sufficient e.m.f. (field current motion-induced stator voltage) to turn off the CSI thyristors is available only above 5% of rated speed.

14.7. RECTIFIER-CSI-SM DRIVE - STEADY-STATE WITH LOAD COMMUTATION

Let us consider that the machine is running above five percent of rated speed. Therefore, sufficient e.m.f. is provided by the field current to produce safe load commutation. By commutation, we mean the turning on and off process of current in the motor phases. Ideally, the d.c. link current is constant in time (because of a high filter inductance L_f). Thus the inverter distributes the d.c. link current as 120° current blocks of alternate polarity between the stator phases in pairs. With instantaneous (ideal) commutation, the ideal currents are as shown in Figure 14.11.

As the SM contains inductances, a sudden change in phase currents, as implied by instantaneous commutation (Figure 14.11) is, in fact, impossible.

Intuitively, it follows that the machine will impose some exponential (or almost linear) variation of currents throughout the commutation process. So the actual currents are trapezoidal rather than rectangular.

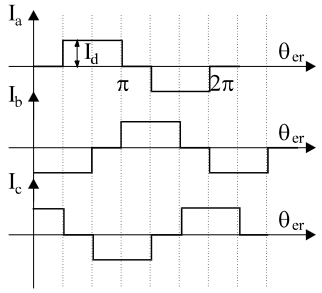

Figure 14.11. Ideal stator current waveforms

As the commutation process is rather fast — in comparison with the current period — the machine behaves approximately according to the voltage behind the subtransient inductance principle (Figure 14.12).

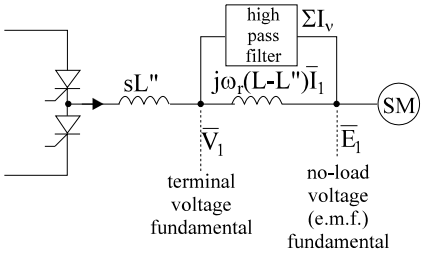

Figure 14.12. Equivalent circuit under mechanical steady-state

The voltage behind the subtransient inductance L″, V_1, is, in fact, the terminal voltage fundamental if phase resistance is neglected. The no-load (e.m.f.) voltage E_1 is also sinusoidal. The space vector (or phasor) diagram may be used for the current fundamental I_1 for L–L″ with L as synchronous inductance and L″ the subtransient inductance along the d-q axes (Figure 14.13) [7].

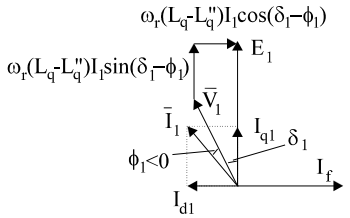

Figure 14.13. Space vector (or phasor) diagram for the voltage behind subtransient inductance

$$V_1 \cos\delta_1 = E_1 - \omega_r\left(L_d - L_d''\right) I_1 \sin\left(\delta_1 - \phi_1\right) \tag{14.30}$$

$$V_1 \sin\delta_1 = \omega_r\left(L_q - L_q''\right) \cdot I_1 \cos\left(\delta_1 - \phi_1\right) \tag{14.31}$$

In general, the machine may have salient poles ($L_d \neq L_q$) and, definitely, damper windings ($L_d'' << L_d$, $L_q'' << L_q$). The currents induced in the damper windings due to the nonsinusoidal character of stator currents are neglected here.

During commutation intervals the machine reacts with the subtransient inductance. An average of d-q subtransient inductances L_d'' and L_q'' is considered to represent the so-called commutation inductance L_c given by

$$L'' = L_c \approx \frac{1}{2}\left(L_d'' + L_q''\right) \tag{14.32}$$

14.7.1. Commutation and steady-state equations

To study the commutation process let us suppose that, at time zero, phases a and c are conducting (Figure 14.14) (T_1T_2 in conduction)

$$\text{at } t = 0 \;\; I_a = +I_d, \;\; I_c = -I_d \text{ and } I_b = 0 \tag{14.33}$$

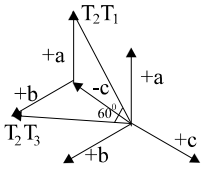

Figure 14.14. Stator m.m.f. (60° jump from T_1T_2 to T_2T_3 conduction)

The advance angle control requires a jump of 60° counterclockwise in the stator current space vector. That is, leave −c conducting and switch phase +a for +b with T_2T_3 (after T_1T_2).

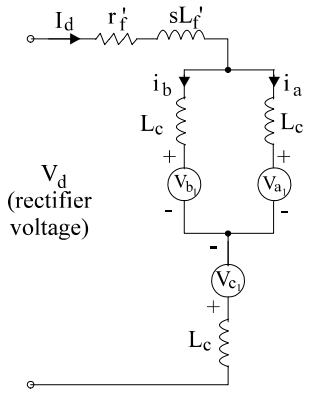

Figure 14.15. Equivalent circuit for commutation

During this commutation process phases +a and +b are both conducting (in parallel) with phase −c continuing conduction (Figure 14.15).

The loop made of phases a, b in parallel (Figure 14.15) has the equation

$$L_c \frac{di_a}{dt} + V_{a1} = L_c \frac{di_b}{dt} + V_{b1} \tag{14.34}$$

$$i_d = i_a + i_b \tag{14.35}$$

At the end of the commutation interval ($t = t_c$), phase b is conducting

$$i_a = 0, \;\; i_b = I_d \;\; \text{for} \;\; t = t_c \tag{14.36}$$

The fundamental voltages V_{a1} and V_{b1}, represent, as explained above, voltages behind transient inductances and are thus considered sinusoidal in time.

Eliminating i_b from (14.34)-(14.35) yields

$$2L_c \frac{di_a}{dt} = -\left(V_{a1} - V_{b1}\right) \tag{14.37}$$

For successful commutation, the current in phase a should decrease to zero during the commutation interval ($di_a/dt < 0$). Consequently, the line voltage V_{ab1} should necessarily be positive when the current switches from phase +a to phase +b (Figure 14.16).

If the commutation process is triggered sufficiently before V_{ab1} goes to zero, from positive values, the phase a current i_a will be driven to zero.

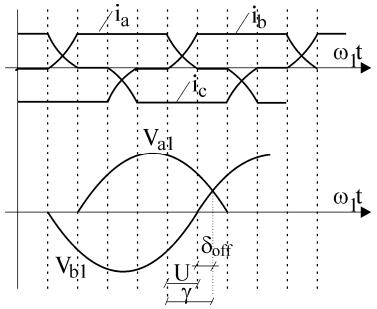

Figure 14.16. The commutation process

Before V_{ab1} goes to zero, a time interval t_{off} (δ_{off} / ω_r) is required with $i_a = 0$ to allow the recombination of charges in the thyristor T_1.

According to Figure 14.16 the phasing of V_{ab1} is

$$V_{ab1} = V_{a1} - V_{b1} = -V_1\sqrt{6}\sin\left(\omega_r t - \gamma\right); \;\; 0 < \omega_r t < \gamma \tag{14.38}$$

with V_1 the rms value of phase voltage fundamental. Integrating (14.38) from $t = 0$ to $t_c = u / \omega_r$, we obtain

$$V_1\sqrt{6}\left(\cos\left(\gamma - u\right) - \cos\gamma\right) = 2L_c I_d \omega_r \tag{14.39}$$

The angle u corresponds to the overlapping time of currents i_a and i_b. For $I_d = 0$, $u = 0$ and γ should be greater than u for successful commutation. Ideally, $\gamma - u = \delta_{off}$ should be kept constant so both γ and u should increase with current.

It is now clear (as $\gamma_{max} = 60°$) that the maximum current commutated safely is inversely proportional to the commutation inductance L_c. The lower L_c the better, *so a damper winding in the rotor is necessary*.

The rms phase current fundamental is related to the d.c. current I_d by

$$I_1 \approx \frac{\sqrt{6}}{\pi}\frac{\sin(u/2)}{(u/2)} I_d \approx \frac{\sqrt{6}}{\pi} I_d \tag{14.40}$$

and was obtained by using the trapezoidal current shape of Figure 14.16. The power factor angle ϕ_1 between V_1 and I_1 (Figure 14.17) is approximately [7]

$$\phi_1 \approx \gamma - u/2 \tag{14.41}$$

The inverter voltage V_I is made of line voltage segments disturbed only during the commutation process

$$V_I(t) = V_{a1}(t) - V_{c1}(t); \quad 0 \le \omega_r t \le (\pi/3 - u) \tag{14.42}$$

$$V_I(t) = V_{a1}(t) - V_{c1}(t) + L_c \frac{di_a}{dt}; \quad (\pi/3 - u) \le \omega_r t \le \pi/3 \tag{14.43}$$

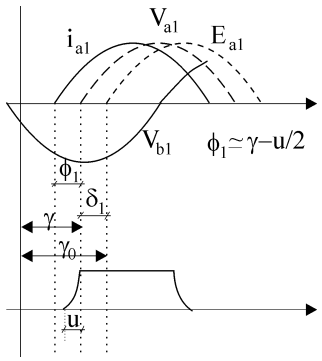

Figure 14.17. Fundamental phase current and voltage phasing

Finally, making use of (14.37)-(14.43), we obtain the average inverter voltage V_{Iav}

$$V_{Iav} = \frac{3}{\pi}\int_0^{\pi/3} V_I(t)\,d(\omega_r t) = \frac{3}{\pi}\left(V_1\sqrt{6}\cos\gamma - L_c I_d \omega_r\right) \tag{14.44}$$

So the commutation process produces a reduction in the motor terminal voltage V_1 by $L_c I_d \omega_r$ for a givenV_{Iav}.

Neglecting the power losses in the CSI and in the motor

$$I_{dc}V_{Iav} = 3V_1I_1\cos\varphi_1 = T_{eav}\cdot\frac{\omega_r}{p};\ \ I_1 = I_d\frac{\sqrt{6}}{\pi} \tag{14.45}$$

As expected, the simultaneous torque $T_e(t)$ is

$$T_e(t) = \frac{I_{dc}V_I(t)}{\omega_r / p} \tag{14.46}$$

Consequently, the torque pulsates as does the inverter voltage (Figure 14.18).

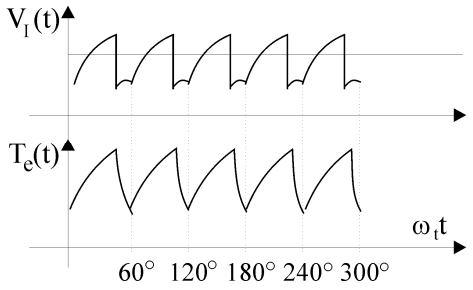

Figure 14.18. Inverter voltage $V_I(t)$ and motor torque pulsations during steady-state

The torque pulsations in Figure 14.18 are different from voltage pulsations during commutation periods especially due to the filtering effect of the motor rotor damper winding.

14.7.2. Ideal no-load speed

To calculate the ideal no-load speed (zero I_d, zero torque), we have to use all equations in this section (from (14.30)-(14.31)) to obtain

$$\delta_1 = 0,\ V_1 = E_1,\ \ u = 0,\ \gamma = \gamma_0;$$
$$V_1 = L_{dm}I_F\omega_{r0} / \sqrt{2} \tag{14.47}$$

Finally, from (14.39)-(14.44)

$$\omega_{r0} = \frac{V_{Iav0}\pi}{3\sqrt{3}L_{dm}I_F\cos\gamma_0} \tag{14.48}$$

Also, the rectifier voltage V_r is related to inverter voltage V_I

$$V_{rav} = V_{Iav} + r_rI_d = V_{Iav};\ (I_d = 0) \tag{14.49}$$

14.7.3. Speed control options

To vary speed, we need to vary the ideal no-load speed. The available options are:

- inverter voltage variation through rectifier voltage variation up to maximum voltage available;
- reducing the field current i_F (flux weakening);
- modify the control angle γ_0. As γ_0 may lay in the 0 to 60° interval, this method is not expected to produce significant speed variations. However varying γ (or γ_0) is used to keep the power factor angle ϕ_1 rather constant ($\phi_1 \approx \gamma - u/2$) or δ_{off} = cons. for safe commutation.

Example 14.1. A rectifier-CSI-SM drive is fed from a V_L = 4.8 kVa.c. (line to line, rms), power source, the magnetization inductance L_{dm} = 0.05H and rated field current (reduced to the stator) i_{Fn} = 200A.

Determine:

- The maximum average rectifier voltage available;
- The ideal no-load speed ω_{r0} for $\gamma_0 = 0$;
- For $L_c / L_{dm} = 0.3$, $\gamma = 45^0$ and I_d = 100A, $\omega_r / \omega_{r0} = 0.95$, calculate the fundamental voltage V_1 and the overlapping angle u.

Solution:

The fully controlled rectifier produces an average voltage V_r (Chapter 5, equations (5.54)).

$$V_r = \frac{3V_L\sqrt{2}}{\pi}\cos\alpha \tag{14.50}$$

So
$$V_{r\,max} = \frac{3\cdot 4800\sqrt{2}}{\pi}\cdot 1 = 6466 \text{ V} \tag{14.51}$$

The ideal no-load speed (14.48) is

$$\omega_{r0} = \frac{6466\cdot\pi}{3\sqrt{3}0.05\cdot 200\cdot 1} = 390 \text{ rad/s} \tag{14.52}$$

The voltage fundamental V_1 becomes (14.44)

$$V_1 = \frac{6646\cdot\pi/3 + 0.95\cdot 390\cdot 0.3\cdot 0.05\cdot 100}{\sqrt{6}\cdot\cos 45^0} = 4336 \text{ V} \tag{14.53}$$

Now, from (14.39) the overlapping angle u is found

$$4336\sqrt{6}\left(\cos(\gamma - u) - \cos\gamma\right) = 2\cdot 0.3\cdot 0.05\cdot 390\cdot 0.95\cdot 100 = 1111.5$$
$$\cos(\gamma - u) = 0.807; \quad u = 4.8° \tag{14.54}$$

The overlapping angle u is small, indicating an unusually strong damper winding. Higher values of u are practical.

14.7.4. Steady-state speed/torque curves

By now we know that the rectifier-CSI-SM drives exhibit a finite ideal no-load speed much like d.c.-brush motors with separate excitation.

However, it is important if the speed increases or decreases with torque for given inverter voltage V_{Iav}. An increase of speed with torque means an unstable speed/torque characteristic while speed decreasing with torque means a statically stable characteristic.

While successful commutation has to be provided up to the maximum load torque considered, the drive may work with γ_0 = cons. (direct position sensor required) or with ϕ_1 = cons. = γ–u / 2.

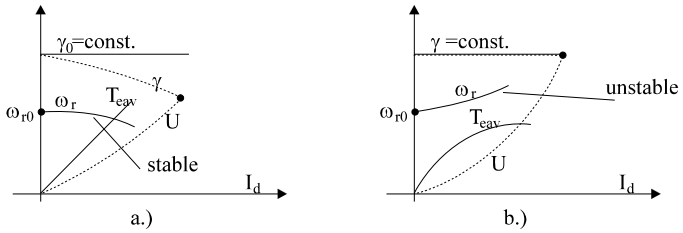

Figure 14.19. Steady-state curves (V_{Iav} = cons., i_F = cons.): a.) for constant γ_0 (position sensor); b.) for constant γ (terminal voltage zero crossing angle).

The above relationships suffice to calculate the ideal motor speed/torque (I_d) curves and the variation of overlapping angle u with load (I_d).

For γ_0 = cons. the speed / torque curve proves to be stable (Figure 14.19a). This is not the case for γ = cons. (Figure 14.19b).

So far, the field current was considered constant with load (I_d). If the field current increases with load to keep the power factor constant (ϕ_1 = cons. = γ–u/2), it means that we should increase γ with load as (anyway) the overlapping angle u does so (Figure 14.19). This way the speed will decrease with load and thus, as a bonus, static stability is restored (Figure 14.20).

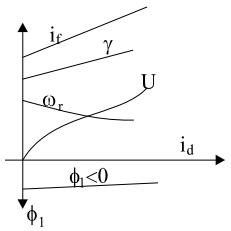

Figure 14.20. Steady-state curves (V_{Iav} = cons.), i_F - variable, ϕ_1 = cons. = γ–u / 2

Results in Figure 14.20 lead naturally to the conclusion that, for high performance variable speed control, both the angle γ and field current i_F

should increase with load to secure constant power factor and safe commutation. These conclusions will be fully exploited in the dynamics and control section later in this chapter.

14.7.5. Line commutation during starting

As already mentioned, at low speeds (below 5% of rated speed), the e.m.f. is not high enough to produce a leading power factor ($\phi_1 < 0$) and thus secure load commutation (the resistive voltage drop is relatively high). For starting either line commutation or some forced commutation (with additional hardware) [4] is required.

To start, the angle $\gamma(\gamma_0)$ is chosen to be zero to obtain maximum torque per ampere. When the commutation of phases is initiated, both thyristors conducting previously are first turned off by applying a negative voltage at the machine terminals through increasing the rectifier delay angle to about 150°-160°. To speed up the d.c. link current attenuation to zero, the d.c. choke is short-circuited through the starting thyristor (Figure 14.10).

Current notches occur and thus the torque pulsations may also be slightly reduced, while the motor accelerates smoothly.

14.7.6. Drive control loops

While the basic scheme of the control system remains the same as in Figure 14.10, we will briefly discuss some practical solutions for speed, ω_r, current, I_d, advance angle (γ) and field voltage control.

A typical speed controller capable of providing for safe load commutation during the transients is shown in Figure 14.21. The d.c. link current controller, the reference angle γ^* and the field current voltage V_f^* are all included.

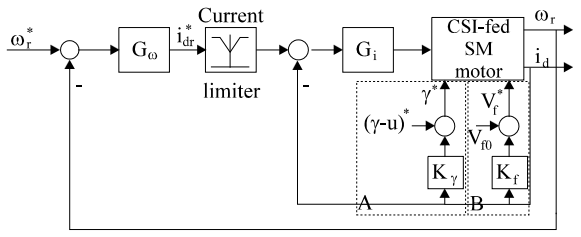

Figure 14.21. Speed control system (rectifier-CSI-SM drive)

A PI speed controller is, in general, used

$$I_d^* = \left(\omega_r^* - \omega_r\right) G_\omega \tag{14.55}$$

with

$$G_\omega = K_{c\omega}\left[1 + 1/T_{i\omega}s\right] \tag{14.56}$$

where $K_{c\omega}$ is the gain and $T_{i\omega}$ the integral time constant. Safe load commutation has to be provided, in general, up to 150% of rated current. A current limiter is required. The integral part of the speed controller is thus not desirable during the current limiter saturation period. This may be done by inhibiting the integral part of the current controller, as long as the current is higher than a limit value.

The current controller may also be of PI type

$$V_r^* = G_i\left(I_d^* - I_d\right) \tag{14.57}$$

with

$$G_i = K_{ci}\left[1 + 1/T_{ii}s\right] \tag{14.58}$$

As expected, $T_{ii} << T_{i\omega}$ and, in general, $T_{i\omega} > 4T_{ii}$. The advance angle γ^* will be increased with the load current as suggested in the previous section

$$\gamma^* = (\gamma - u)^* + K_\gamma I_d \tag{14.59}$$

The initial angle $(\gamma - u)^* \approx 15° - 25°$ provides for safety margin as required by slow, standard (low cost) thyristors

$$(\gamma - u)^* \geq \omega_{r\,max} t_{off};\ \ t_{off} = 0.3 - 0.5\text{ms} \tag{14.60}$$

Though this is only a linear (intuitive) approximation, it has been proved practical. As in most CSI-SM drives, fast drive response is not a high priority, a field voltage referencer V_f^* suffices instead of a field current controller

$$V_f^* = V_{f0} + K_f I_d \tag{14.61}$$

This way, a rather constant safety margin angle $(\gamma - u)^*$ with increasing loads and a constant power factor (leading power factor angle $\phi_1 = -(8°\text{-}10°)$) are obtained. For control numerical details related to a practical case, see [8]. Such drives are, by now, standard in industry for powers up to 30MW (5500rpm) per unit [9].

To improve (speed up) the current response at high speeds, an e.m.f. V_c compensator may be added to the d.c. link current controller. The e.m.f. may be based on the flux λ" behind the commutation inductance L_c

$$\bar{\lambda}'' = \int\left(\bar{V}_s - r_s\bar{i}_s\right)\cdot dt - L_c\bar{i}_s \tag{14.62}$$

$$V_c = \left|\bar{V}_c\right| = \left|j\omega_r\lambda''\right| \tag{14.63}$$

Above 5% of rated speed, the $\bar{\lambda}''$ calculator is good enough even if based only on the voltage model.

Feedforwarding the value of the V_c to the d.c. link current controller produces notable increases in the current response quickness. The above control system - in fact, of indirect vector current type - looks rather simple but relies heavily on known machine data and parameters.

A more direct, robust approach, such as direct vector control, has also been proposed [10].

As an alternative to this concept, the DTFC principle is introduced here.

14.7.7. Direct torque and flux control (DTFC) of rectifier-CSI-SM drives

As the stator current is rather trapezoidal, the stator flux is nonsinusoidal even under steady-state. The subtransient flux linkage λ'', defined above, is however, very close to a traveling wave during steady-state. For DTFC, we thus make use of λ''. A tentative DTFC configuration is shown in Figure 14.22.

The CSI provides 6 nonzero current space vectors $\bar{I}_{1,...,6}$ produced by 2 phases conducting at any time outside the commutation zones (Figure 14.23.)

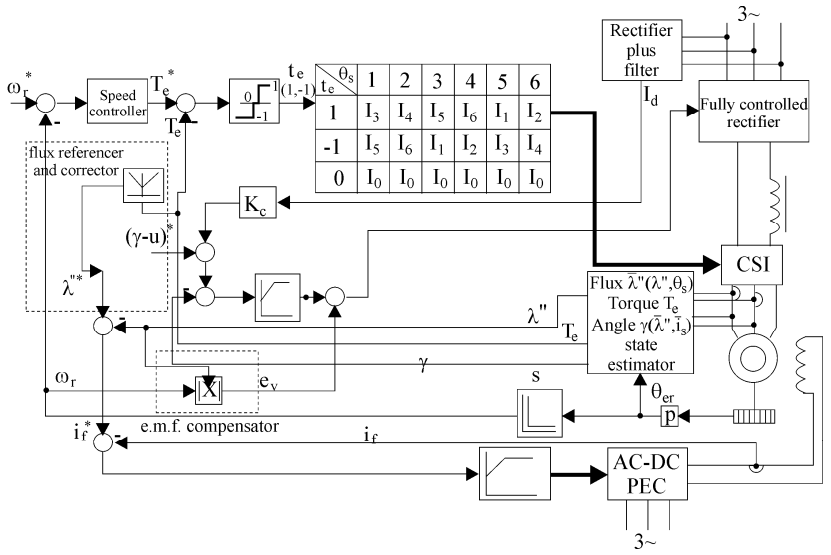

Figure 14.22. Tentative DTFC system for CSI-SM drives

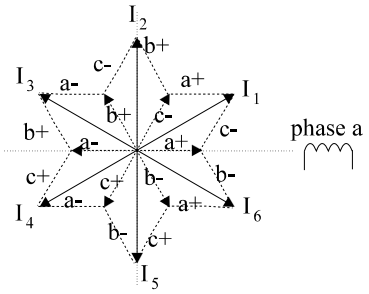

Figure 14.23. CSI-current space-vectors

The subtransient flux λ'' position in one of the 6 sectors (Figure 14.23) is used to select the required current space vector, depending also on the torque error sign. As the machine is overexcited, the forthcoming current vector should be located at an angle greater than 90° with respect to the $\bar{\lambda}''$ position. So for $\bar{\lambda}''$ in the first sector (0° to 60°), I_3 should be applied for positive torque error and I_5 for negative torque error.

A hysteresis angle may be allowed at the boundary between sectors to reduce the switching frequency. The hysteresis band of the torque controller may be increased with speed to avoid PWM of current at high speeds.

For zero torque error the thyristors of upper and lower lag of a phase are applied such that to minimize the switching frequency of the thyristors. In fact the current (I_0) in the machine is zero, but the a.c. choke limits the d.c. link current.

The subtransient flux estimator could be built in many ways. A combination of voltage (14.62) and current model is the obvious way to build a wide speed range subtransient flux estimator. Sensorless control may also be considered but a speed estimator is additionally required.

14.8. SUB- AND HYPER-SYNCHRONOUS IM CASCADE DRIVES

14.8.1. Limited speed control range for lower PECs ratings

Limited speed control range is required in many applications such as high power pumps, fans, etc. Low motor speed range control, (20-30% around rated speed) implies frequency control.

Stator frequency control, in either SMs or IMs, no matter the speed control range, requires full motor power PECs. So it is costly for the job done. It is very well known that the power balance in the wound rotor of IMs is characterized by the slip formula

$$SP_{elm} = P_{Co2} + P_r;\quad S = \frac{\omega_1 - \omega_r}{\omega_1};\quad \omega_1 = 2\pi f \tag{14.64}$$

where P_{elm} is the electromagnetic (active) power that "crosses the airgap", or is exchanged between rotor and stator in IMs; P_{Co2} is the rotor winding loss and P_r is the electric active power extracted or introduced (injected) into the rotor.

Neglecting, for the time being, the rotor winding loss ($P_{Co2} = 0$), the electric power injected into the rotor at slip frequency $f_2 = Sf_1$ is

$$P_r \approx SP_{elm} = \frac{\omega_1 - \omega_r}{\omega_1} P_{elm} \tag{14.65}$$

The speed control range is defined through the minimum speed, ω_{rmin}, or the maximum slip, S_{max},

$$S_{max} = \frac{\omega_1 - \omega_{rmin}}{\omega_1} \tag{14.66}$$

So the maximum active electric power injected in the wound rotor is

$$P_{r\,max} \approx S_{max} P_{elm} \tag{14.67}$$

For a 20% speed control range $S_{max} = 0.2$ and thus the PEC required to handle the rotor injected power P_{rmax} is rated to S_{max}, that is 20%-30% of motor rated power.

In general, as the rotor voltage required at low slip frequency $f_{2max} = S_{max}f_1$ is low, a step-up transformer is mandatory to exchange energy with the power grid also used to feed the stator windings (Figure 14.24).

In essence, P_r may be positive or negative and thus sub- or hyper-synchronous operation is feasible, but the rotor side PEC has to be able to produce positive and negative sequence voltages as

$$f_1 = f_2 + \frac{\omega_r}{2\pi}; \quad f_2 = Sf_1 \gtrless 0 \tag{14.68}$$

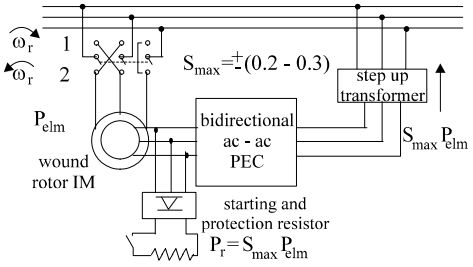

Figure 14.24. Sub- and hyper-synchronous IM cascade system

For $S < 0$, $f_2 < 0$ and thus negative sequence voltages are required. As the machine is reversible, both motoring and generating should be feasible,

provided that a bidirectional power flow is allowed for through the rotor side PECs.

Also, a smooth transition through S = 0 is required. For S = 0 (stator produced synchronism) $f_2 = 0$ and thus d.c. current (m.m.f) should be injected into the rotor. These challenging constraints restrict the types of PECs to be used for direct a.c.-a.c. conversion.

Cyclo or matrix converters and two "back to back" voltage source PWM inverters are adequate for the scope.

Note: The so-called slip-recovery scheme is simple but, allowing only unidirectional power flow (from machine rotor to power grid), may work only as a subsynchronous motor (or as a hypersynchronous generator). On top of that the total power factor of the machine is notably low. This is the reason why we do not treat it here.

Let us note that the sub- and hyper-IM cascades may work both as a motor and a generator above and below f_1 / p and thus are used for pumped storage power plants. In this latter case, for motoring, the turbine will have, in general, to change the direction of motion to act as a pump. This explains the presence of a power switch 1-2 (Figure 14.24). Also, to protect the rotor side converter from overvoltages or overcurrents "induced" by stator faults (short-circuits, etc.) and for starting, a controlled resistor is introduced at the rotor terminals (Figure 14.24).

14.8.2. Sub- and hyper-operation modes

The induction machine equations in stator field (synchronous) coordinates are (Chapter 8, equations (8.50)-(8.52))

$$\overline{V}_s = r_s \bar{i}_s + \frac{d\overline{\lambda}_s}{dt} + j\omega_1 \overline{\lambda}_s \tag{14.69}$$

$$\overline{V}_r = r_r \bar{i}_r + \frac{d\overline{\lambda}_r}{dt} + jS\omega_1 \overline{\lambda}_r \tag{14.70}$$

$$\overline{\lambda}_s = L_s \bar{i}_s + L_m \bar{i}_r;\ \overline{\lambda}_r = L_r \bar{i}_r + L_m \bar{i}_s \tag{14.71}$$

$$T_e = \frac{3}{2} p\, Re\left(j\overline{\lambda}_s \bar{i}_s^*\right) = -\frac{3}{2} p\, Re\left(j\overline{\lambda}_r \bar{i}_r^*\right) \tag{14.72}$$

In the cascade configuration, the rotor circuits are fed with three-phase voltages (and currents) represented by the space vector $\overline{V}_r$.

Note that $\overline{V}_r$ and $\bar{i}_r$ in equations (14.69-14.70) are referred to the stator and expressed in synchronous coordinates. During steady-state $\overline{V}_r$, $\bar{i}_r$

represent quantities at stator frequency ω_1, while in the real machine their frequency is $\omega_2 = S\omega_1$.

For steady-state (d/dt = 0) equation (14.70) becomes

$$\bar{V}_r = r_r \bar{i}_r + jS\omega_1 \bar{\lambda}_r \tag{14.73}$$

The ideal no-load speed ω_{r0} is obtained for zero rotor current

$$\bar{V}_r = j(\omega_1 - \omega_{ro})\bar{\lambda}_r \tag{14.74}$$

From (14.69) with $\bar{i}_r = 0$ and d/dt = 0

$$\bar{V}_s = r_s \bar{i}_{s0} + j\omega_1 L_s \bar{i}_{s0}; \quad \bar{\lambda}_{r0} = L_m \bar{i}_{s0} \tag{14.75}$$

Neglecting r_s ($r_s = 0$)

$$\bar{\lambda}_{r0} = \bar{\lambda}_{s0} \cdot \frac{L_m}{L_s} = \frac{\bar{V}_s}{j\omega_1} \frac{L_m}{L_s} \tag{14.76}$$

From (14.74) with (14.76)

$$\bar{V}_{r0} = \bar{V}_{s0} \cdot S\omega_1 \frac{L_m}{L_s} \tag{14.77}$$

For ideal no-load, the stator and rotor voltages (in synchronous coordinates) are, for steady-state, d.c. quantities. They may be written as

$$V_{r0} = V_{s0}\left(\frac{\omega_1 - \omega_{r0}}{\omega_1}\right)\frac{L_m}{L_s} \tag{14.78}$$

$$\omega_{r0} = \omega_1\left(1 - \frac{V_{r0}}{V_{s0}}\frac{L_s}{L_m}\right) \tag{14.79}$$

For $V_{ro} > 0$ (zero phase shift) and $V_{s0} > 0$, $\omega_{r0} < \omega_1$ and subsynchronous operation is obtained. In contrast, for $V_{r0} < 0$ (180° phase shift) (and $V_{s0} > 0$), $\omega_{r0} > \omega_1$, the hypersynchronous operation is obtained.

On the other hand, multiplying (14.73) by $3/2\bar{i}_r^*$ and extracting the real part, we obtain

$$P_{rotor} = \frac{3}{2}\mathrm{Re}\left(\bar{V}_r \bar{i}_r^*\right) = \frac{3}{2} r_r i_r^2 - S\frac{\omega_1}{p_1} T_e \tag{14.80}$$

As known, $\omega_1 T_e / p_1 = P_{elm}$ is the electromagnetic (airgap) power transferred through the airgap from stator to rotor

$$P_{rotor} = \frac{3}{2} r_r i_r^{\ 2} - SP_{elm} \tag{14.81}$$

It is now clear that we may have $P_{elm} > 0$ (motoring) or $P_{elm} < 0$ (generating) for both positive and negative slips, that is subsynchronous and hypersynchronous operation, provided that the active electric power injected in the rotor P_{rotor} may be either positive or negative.

The definition of slip frequency ω_2

$$\omega_2 = \omega_1 - \omega_r = S\omega_1 \tag{14.82}$$

Equation (14.82) shows that for $S < 0$ ($\omega_r > \omega_1$), $\omega_2 < 0$, that is the phase sequence in the rotor is inverse with respect to the stator.

Also multiplying (14.73) by $3/2 i_r^*$, but extracting the imaginary part, we obtain

$$Q_{rotor} = \frac{3}{2} Imag\left(\overline{V}_r \bar{i}_r^{\,*}\right) = S\omega_1 \frac{3}{2} Imag\left(j\overline{\lambda}_r \bar{i}_r^{\,*}\right) \tag{14.83}$$

Neglecting the stator resistance and replacing $\overline{\lambda}_s$ with $\overline{\lambda}_r$ in (14.69) we may obtain, after multiplication with i_s^* (and $\bar{i}_s = -\bar{i}_r$; $\overline{\lambda}_r \approx \overline{\lambda}_s - L_{sc}\bar{i}_s$; $\overline{V}_s = j\omega_1 \overline{\lambda}_s$)

$$Q_1 = \frac{3}{2} Imag\left(\overline{V}_s \bar{i}_s^{\,*}\right) = \frac{3}{2}\omega_1 L_{sc} i_s^{\ 2} - \frac{Q_{rotor}}{|S|} \tag{14.84}$$

So, if reactive power is injected in the rotor, it will be subtracted from the reactive power injected in the stator. Eventually, leading power factor ($Q_1<0$) in the stator is obtained at the cost of lagging power factor in the rotor. If the PEC on the rotor side itself is capable — through capacitors — of producing Q_{rotor}, then the total power factor may be close to unity or even slightly leading. However, as the rotor voltage is rather low, this is hardly a practical way to produce reactive power through capacitors.

On the other hand, the rotor side PEC may be of a voltage source or current source type. It seems that rotor voltage control leads to motor-only stable operation in the subsynchronous mode and to generator-only in the hypersynchronous mode. For rotor current control, both motoring and generating are stable in sub- and hyper-synchronous modes [11].

14.8.3. Sub- and hyper-IM cascade control

The power structure of the sub- and hyper-IM cascade drive is as shown in Figure 14.24. The control system is related to controlling the speed and, eventually, the stator reactive power for motoring and active and reactive stator power for generating.

As the electromagnetic power P_{elm} is obtained at fixed stator frequency, the torque T_e is

$$T_e = \frac{P_{elm}}{\omega_1} p \tag{14.85}$$

But the torque may be estimated from stator flux as

$$T_e = \frac{3}{2} p \, \mathrm{Re}\left(j\bar{\lambda}_s \bar{i}_s^{\,*} \right) = \frac{3}{2} p \lambda_s i_{sT} \tag{14.86}$$

Now we may define for the stator a "reactive torque"

$$T_{Q_1} = \frac{Q_1}{\omega_1} \tag{14.87}$$

$$T_{Q_1} = \frac{3}{2} \mathrm{Im\,ag}\left(j\bar{\lambda}_s \bar{i}_s^{\,*} \right) = \frac{3}{2} \lambda_s i_{sQ} \tag{14.88}$$

$$\left(\bar{i}_s \right)_{ref} = i_{sT} - j i_{sQ} \tag{14.89}$$

As the value of $f_1(\omega_1)$ is rather large, the stator flux estimation may be performed through the voltage model

$$\bar{\lambda}_s = \int \left(\bar{V}_s - r_s \bar{i}_s \right) dt + \bar{\lambda}_{s0} \tag{14.90}$$

$$\bar{\lambda}_s \approx \left(\bar{V}_s - r_s \bar{i}_s \right) \frac{T_c}{1 + sT_c} + \bar{\lambda}_{s0} \tag{14.91}$$

In essence, the reference stator current $\left(\bar{i}_s \right)_{ref}$ has to be reproduced through the control system. What we need to control, in fact, is the rotor current $\left(\bar{i}_r \right)_{ref}$

$$\left(\bar{i}_r \right)_{ref} = -\left(\bar{i}_s \right)_{ref} - j\bar{I}_\mu = -i_{sT} - j\left(I_\mu - I_{sQ} \right) \tag{14.92}$$

where $\bar{I}_\mu$ is the main flux magnetizing current. Only approximately

$$\bar{I}_\mu = \frac{\bar{\lambda}_s}{L_s} \tag{14.93}$$

$\left(\bar{i}_r \right)_{ref}$ is still in synchronous coordinates. It has to be transformed into rotor coordinates

$$\left(\bar{i}_r \right)^r_{ref} = e^{-j\left(\theta_{cr} - \omega_1 t \right)} \left| \left(\bar{i}_r \right)_{ref} \right| \tag{14.94}$$

So we need a rotor position sensor. Once the reference rotor current is known, a.c. current controllers PWM may be used in the rotor side PEC to produce sinusoidal currents at slip frequency $S\omega_1$.

Note: The rotor position angle θ_{er} and rotor speed considered as measured here, may be estimated and thus a motion sensorless drive is obtained.

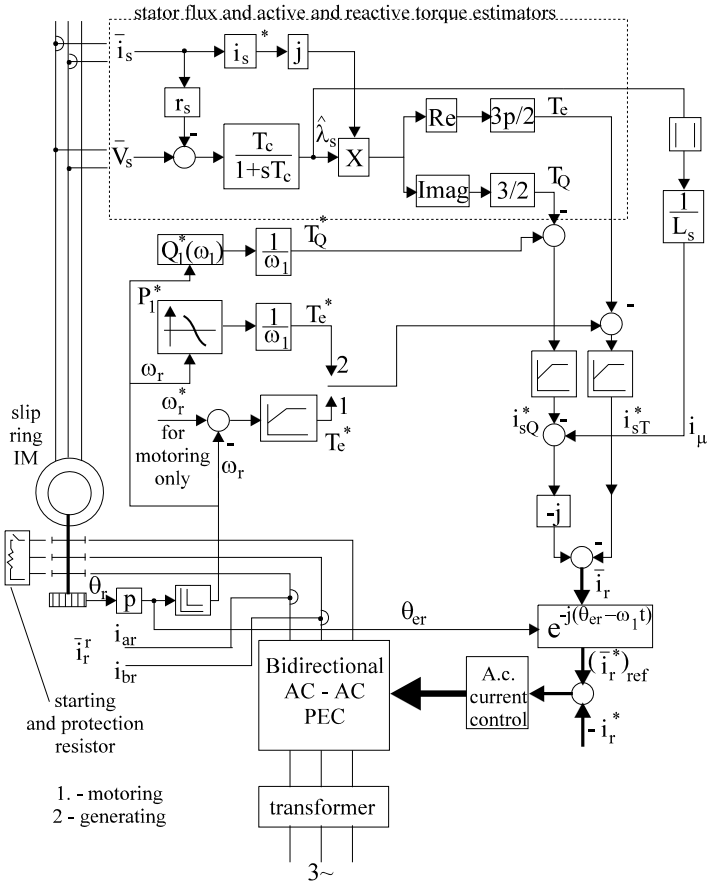

Figure 14.25. Fixed stator frequency motor-generating control with sub- and hyper-synchronous IM cascade

Figure 14.25 summarizes the controller just described for both options — motoring and generating — with independent stator torque or reactive power (torque) control.

For generating, the stator active power input has to be commanded but, again (with ω_1 = cons.), the reference torque T_e^* may be calculated, so the

motor and generating control is similar. Regenerative braking is considered in the drive control mode.

The stator reactive power Q_1 is transformed into a reactive power reference torque T_Q^*. In fact, the active (torque) i_{sT} and reactive i_{sQ} stator current components are proportional to P_{elm} and Q_1 as the stator flux λ_s is constant.

The control system requires a rotor position sensor (resolver, for example) or a rotor position observer if sensorless control is targeted.

For starting, the PEC in the rotor has to be separated from the rotor as high voltages and currents occur. Note that the PEC is designed for 20%-30% of machine full power (and voltage). Alternatively, the drive may be started from rotor side with shortcircuited stator. Then the stator is opened and the conditions for selfsynchronization are quickly provided at variable speed (within the slip speed range). After selfsynchronization loading may be performed.

It also has been shown [4] that current faults (short-circuits) in the stator produce overvoltages in the rotor. Stator voltage variations induce rotor overcurrents. In all these situations, the starting resistors may be connected for protection purposes.

The sub- and hyper- IM cascade represents a rather generalized (unified) solution for limited variable speed motoring and generating applications.

While pumped storage hydropower plants of various powers (up to 400MW/unit, in principle) are the obvious applications, there are other industrial plants where such systems are performance-cost competitive.

Transient behaviour for motor operation mode of such a doubly fed induction machine with vector control in a 400 MW pump – storage power plant at Ohkawachi (Japan) [14] is shown in Figure 14.26.

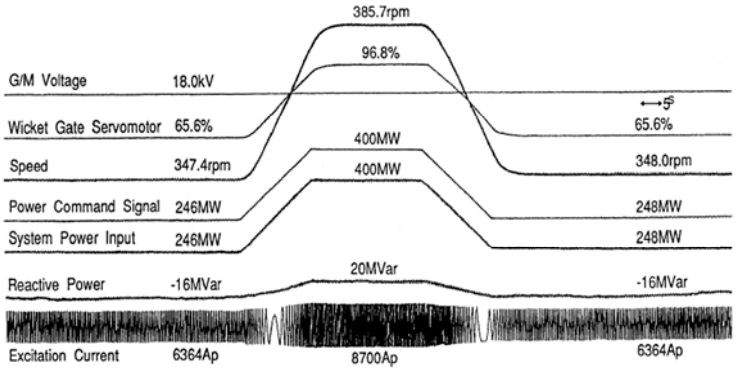

Figure 14.26. 400 MW unit doubly fed induction machine motoring transient with smooth passage through conventional synchronous speed

The smooth passage through the conventional synchronous speed ($n_1=f_1/p$) is evident, together with fast active power (torque) response and small variation of reactive power. This particular case apparently refers to the largest power electric motor drive so far.

14.9. SUMMARY

- High power means power levels beyond the reach of IGBT PWM converters. This limit goes up by the year and it is now (2005) about 6MW.
- GTOs and thyristors are the standard SCRs used in large power industrial drives. But IGCTs are catching on.
- Representative converters for large power may be of voltage source type or current source type.
- 3-level GTO (IGCT) 2-stage PWM a.c.-a.c. voltage source converters for high speeds and cycloconverters (for low speeds) represent the current controlled voltage source type and are used with cageless SMs.
- Phase-delay rectifier current source inverters are of the current source type and are used with cage-rotor SMs.
- Vector current control at unity power factor - indirect or direct version - is used to control the current in the voltage source type a.c.-a.c. converter SM drives.
- E.m.f. compensation or voltage decoupler may be added for better response at high speeds.
- DTFC (direct torque and flux control) may be used for voltage source a.c.-a.c. PECs for a simpler and more robust system.
- Phase delay rectifier-current source inverter SM drives have a low input power factor at low speeds (due to the rectifier) though the CSI is load (e.m.f.) commutated as the SM works with the leading constant power factor. Both vector current control and DTFC systems are feasible for such drives. There are methods to improve input (line) power factor and reduce line current harmonics.
- For limited speed control range (±(20-30%)) wound-rotor IMs are provided with a rotor side PEC and, eventually, a step-up transformer to the power grid.
- The sub- and hyper-synchronous IM cascade, suitable for limited speed control (20-30%), requires a starting and protection resistor, other than the transformer and a.c.-a.c. converter on the rotor side.
- The cyclo or matrix converters can handle motoring and generating modes both sub- and hyper-synchronously (below and above conventional synchronous speed ω_1 (stator frequency)).
- Though the rotor side converter can handle bidirectional reactive power flow, the total power factor of the system is, in general, slightly lagging (unless larger capacitor filter in the d.c. link is added).

- As expected, vector current control or DTFC is to be applied to such systems for quick, precise and robust speed (power) control.
- Dual stator winding stators with single-phase short-circuited (nested) winding or anisotropic rotors of adequate pole number combinations, with only one stator winding converter-fed, have been recently proposed for medium power but are still in the laboratories [12,13].

14.10. PROBLEMS

14.1. Unity power factor SM drive: A nonsalient pole large SM motor is fed from a 3-level PWM voltage source inverter at $\omega_r = 376.7$rad/s, p = 2 with a $V_L = 4.6$kV line to line voltage (rms). The motor rated phase current is $I_n = 1000$A (rms), the synchronous inductance is $l_d = l_q = 0.75$(p.u.). The drive works at the unity power factor and the leakage inductance $l_{sl} = 0.17$ for star connection. Neglecting the stator resistance determine:

14.2. The stator flux space vector amplitude;

14.3. For a dq flux angle $\delta = 30^0$ and rated current calculate the i_d, i_q current components;

14.4. The field current i_F and the corresponding torque T_e.

14.5. An IM cascade drive is designed for a ±20% speed control around synchronous speed. With $L_m / L_s = 0.93$ and stator voltage $V_{sn} = 5$kV, (star connection line voltage (rms)) $I_{sn} = 1000$A, $L_{sc} = 0.05V_{sn} / i_{sn}\omega_1$; $\omega_1 = 2\pi 60$rad/s.Determine:

14.6. The rotor voltage V_{r0} (value and sign) - in synchronous coordinates - for $\omega_{r0} = (1\pm 0.2)\omega_1$ at no-load.

14.7. The required reactive power injection to the rotor side for $\omega_r = 0.8\omega_1$ (S = 0.2) to produce unity power factor on stator side.

14.8. The cycloconverter and step-up transformer — on rotor side — rating.

14.11. SELECTED REFERENCES

1. **P.H. Hammond,** A new approach to enhance power quality for medium voltage a.c. drives, IEEE Trans.vol.IA-33, no.1, 1997, pp.202-208.
2. **R.A. Errath,** 15000HP gearless ball mill drive in cement - why not, IEEE Trans.vol.IA-32, no.3, 1996, pp.663-669.
3. **H. Okayama,** Large capacity high performance 3 level GTO inverter system for steel main rolling mill drives, Record of IEEE-IAS, Annual Meeting, 1996, volI., pp.174-179.
4. **H. Stemmler,** High power industrial drives, Proc. IEEE vol.82, nr.8, 1994, pp.1266-1286.
5. **S. Nonaka, Y. Ueda,** A PWM GTO current source converter - inverter system with sinusoidal input and output, Record of IEEE-IAS, 1987, Annual Meeeting, vol.I, pp.247-252.
6. **T. Nakama, H. Ohsawa, K. Endoh,** A high performance cycloconverter-fed synchronous machine drive system, IEEE Trans., vol.IA-20, no.5, 1984, pp.1278-1284.
7. **J. Rosa,** Utilization and rating of machine commutated inverter - synchronous motor

drives, IEEE Trans., vol.IA-15, no.2, 1979, pp.395-404.

8. **S. Nishikata, T. Kataoka,** Dynamic control of a selfcontrolled synchronous motor drive system, IEEE Trans. Vol.IA-20, no.3, 1984, pp.598-604.
9. **M. Miyazaki, et.al.,** New application of thyristor motor drive system, Record of IEEE-IAS, Annual Meeting, 1984, pp.649-654.
10. **L. Boyter, L. Schmidt,** Microprocessor controlled converter fed synchronous motor using subtransient flux model, Record of IEEE, 1990, MIT, Cambridge, Part 2., pp.427-433.
11. **A. Masmoudi, M.B.H. Kamoun and M. Poloujadoff,** A comparison between voltage and current controls of doubly fed synchronous machine with emphasis on steady-state characteristics, Record of ICEM-1996, Vigo-Spain, vol. 3., pp.212-217.
12. **W.R. Brassfield, R. Spee, T.G. Habetler,** Direct torque control of brushless doubly-fed machines, IEEE Trans., vol.IA-32, no.5, 1996, pp.1098-1104.
13. **Y. Liao, L. Xu, Li Zhen,** Design of a doubly fed reluctance motor for adjustable speed drives, IBID, pp.1195-1203.
14. **T. Kawabara, A. Shibuya, H. Furata,** "Design and dynamic response characteristics of 400 MW adjustable speed pump storage unit for Ohkawachi power station", IEEE Trans. Vol. EC – 11, no. 2, 1996, pp. 376-394.